Buffer-gas-cooled ion clouds in a classical Paul trap: Superimposed stability diagrams and trapping capacity investigations

ARTICLE *in* APPLIED PHYSICS B · OCTOBER 2013

Impact Factor: 1.86 · DOI: 10.1007/s00340-013-5657-1

2 AUTHORS, INCLUDING:

G. Werth

Johannes Gutenberg-Universität Mainz

207 PUBLICATIONS **3,281** CITATIONS

Appl. Phys. B (2014) 114:89–98
DOI 10.1007/s00340-013-5657-1

Applied Physics B
Lasers and Optics

Buffer-gas-cooled ion clouds in a classical Paul trap: superimposed stability diagrams and trapping capacity investigations

H. Leuthner · G. Werth

Received: 5 April 2013 / Accepted: 13 September 2013 / Published online: 8 October 2013

Abstract Ion clouds of different species and variable size are stored in a 3D Paul trap and detected after extraction from the trap. We report on measurements of the superimposed stability regions of four simultaneously stored ion species. We determine the operating conditions for trapping capacity under variation of buffer gas pressure and observe space charge shifts for a specific ion in the presence of other elements.

1 Introduction

3D and linear Paul traps are widely used in mass spectrometry, and ample literature is available on their technique and performance [1–4]. The 3D trap is characterized by parameters a and q, defined as

$$a_z = \frac{-8eU_0}{mr_0^2\Omega^2}; \quad q_z = \frac{4eV_0}{mr_0^2\Omega^2}; \quad a_r = -\frac{a_z}{2}; \quad q_r = -\frac{q_z}{2} \tag{1}$$

U_0 and V_0 are the d.c. and a.c. voltages applied to the trap electrodes, respectively, r_0 the ring electrode diameter, m the stored particle's mass and Ω the trap's driving frequency. Within a certain range of the parameters a and q, given by the stability diagram (see [1–4]), theory predicts stable confinement. In first approximation, the particle oscillates harmonically around the trap center with frequencies ω_r and ω_z, depending on a and q.

The theory holds for a single particle in a perfect trap with hyperbolically shaped electrodes. Trap imperfections, caused, e.g., by truncation of the electrodes or misalignments as well as the Coulomb potential when clouds of ions are confined, can be accounted for by a multipole expansion of the trapping potential

$$\phi(\rho,\varphi,\theta) = \phi_0(t)\cdot\sum_{k=0}^{\infty} c_k\left(\frac{\rho}{\rho_0}\right)^k P_k(\cos\theta) \tag{2}$$

with

$$\phi_0(t) = U_0 + V_0\cos\Omega t \quad \text{and the Legendre polynomials} P_k.$$

The higher-order contributions to the quadrupole potential ($k = 2$) lead to modifications of the ion trajectories. In particular, the ion motion becomes unstable when integer multiples of the motional frequencies ω_r and ω_z add up to be on resonance with a multiple of the rf drive frequency Ω of the trap:

$$\begin{gathered} n_r\omega_r + n_z\omega_z = \kappa\Omega \\ \kappa = 0,1,2\ldots \quad n_r,\ n_z = 0,\ \pm1,\ \pm2\ldots \end{gathered} \tag{3}$$

Then, the ion motion is coupled to the trap's driving field and gains sufficient energy to leave the trap. The main contribution to a resonance of the order $N = |n_r| + |n_z|$ arises from the multipole order $k = N$.

This has been theoretically and experimentally investigated in detail by Wang and Franzen [5, 6] and Alheit et al. [7], respectively. Imperfections may also be introduced deliberately, e.g., by different shapes or sizes of the trap′s electrodes and may be used for increased mass resolution [8]. Coupling of additional excitation field with frequency ω_{exc} to the trap electrodes change the right side of Eq. (3) to $\kappa\ \Omega + \kappa_{exc}\omega_{exc}$ with $\kappa_{exc} = 0, \pm 1, \pm 2\ldots$ [7].

For a nonharmonic trap potential, the region where in the ideal case stability of the ion motion is assured contains

H. Leuthner · G. Werth (✉)
Institut für Physik, Johannes Gutenberg Universität Mainz,
55099 Mainz, Germany
e-mail: werth@uni-mainz.de

many lines of instabilities (see [7]). These become particularly pronounced in the region of large values of q. In addition to trap potential unharmonicities instabilities of the ion motion may be caused by external noise having frequency components at one of the ion oscillations. At the position of all these instabilities, the storage time is significantly reduced. In case of experiments with simultaneously stored ions of different charge/mass ratio, the stability diagrams overlap and there is a finite probability that for a given set of trap voltages U_0 and V_0, some of the ion species may fall in a region of reduced stability while others remain stable. Consequently the relative abundances of several simultaneously stored ions with different charge-to-mass ratios depend on the storage time.

In this communication, we report about investigations of the stability behavior in case of several simultaneously stored ion species. We study the influence of buffer gas pressure on the trapping capacity as well as space charge effects on collective resonances. We observe resonant behavior of the ion's oscillation either by excitation from an additional radio-frequency field or without excitation by scanning the trap parameters.

2 Experimental setup and measurements

We use a 3D hyperbolical Paul trap consisting of a ring electrode of 2 cm radius and two separated endcaps. The ratio of the ring radius r_0 and the endcaps closest distance from the trap′s center z_0 is $\sqrt{2}$. Originally designed for a different experiment, the ring electrode has three holes in the center plane, two of them with 8 mm diameter facing each other, whereas the third one (diameter 4 mm) is placed under 90° with respect to them. All trap dimensions have an uncertainty of below 0.2 mm. Ions are created by ionization of the residual gas by an electron beam entering the trap through a hole in the lower endcap. Up to 10^6 ions are trapped, and after a fixed period, the ions are extracted through a mesh-covered hole of 2 cm diameter in the upper endcap. They are accelerated by an rectangular voltage pulse of typically 300 V on the upper endcap that is phase correlated with the trapping field. Typically, we used a phase angle of 135° which gives the maximum ion signal [9]. After leaving the trap, the ions are focussed onto an ion multiplier (Philips XP 1600 series) by an ion optical system. The drift length from the trap center to the multiplier is about 8.5 cm. The trapping frequency Ω is fixed at $2\pi \times 748.8$ kHz, and the trapping voltages applied to the ring electrode can be chosen in a wide range: $-200\ \text{V} \leq U_0 \leq +200\ \text{V}$ and $0\ \text{V} \leq V_0 \leq 1\ \text{kV}$. The endcaps are connected to ground by 100 Ω—resistors. An additional external rf voltage can be applied between endcaps and ring electrode for quadrupole excitation of the ion's motion. The rf drive and the additional external rf source have a combined instability of below 5 Hz.

The trap is enclosed in a stainless steel vessel evacuated by a getter pump. By a variable leak helium or nitrogen can be introduced. The gas pressure is monitored by a quadrupole gas analyser and can be varied between 10^{-5} and 10^{-9} mbar. We use He and N_2 from commercial gas bottles. The resulting buffer gas contains small impurities of O_2, H_2O, CO_2, H_2, N_2 and Ar. Using He, N_2 is the main impurity with a partial pressure up to 1/10 of that of He. With N_2 as buffer gas, O_2 is the main impurity with a similar amount. In both cases, the other gases contribute with partial pressures of 1/20–1/1,000.

A measurement cycle consists of ion creation, trapping and detection. It is controlled via PC. Automatized series of these cycles can be performed while the computer varies one of the following parameters: creation time, storage time, U_0 and V_0. The remaining parameters such as the current of the electron gun or amplitude and phase of the extraction pulse voltage are constant during the measurement cycle and are set manually.

After extraction, different ion species can be distinguished by their different time of flight to the detector. Lighter masses arrive earlier. They can be investigated separately by a timing gate (Fig. 1).

The multiplier output is converted by an analog to digital converter and further handled by PC. The trapped ion number is determined from the output amplitude of the multiplier after calibration of its gain by observation of single ion events at different multiplier voltages. The losses on the ion's path from the trap to the multiplier were determined by a simulation. The quantum efficiency of the ion multiplier was

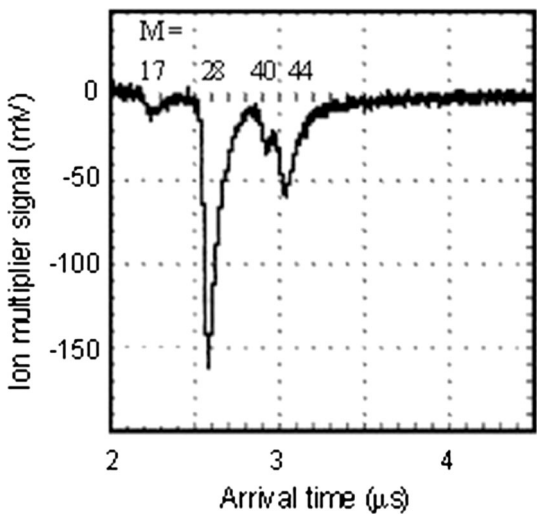

Fig. 1 Arrival time of different simultaneously trapped ions at a detector placed about 8.5 cm from the trap's center after extraction by a high-voltage pulse

considered as stated by the manufacturer. We arrive at an overall detection efficiency of 6.5 ± 2 %.

3 Experimental results

3.1 Superimposed stability regions

By setting a fixed U_0 and an appropriate amplification voltage for the ion multiplier, we make automated measurements at a series of V_0 values, which results in a scan through the stability diagram. After each data point, the trap was empty and new ions were created for the next one. Repeating this in a semi-automated manner for a variety of values of U_0, we obtain a survey of the complete stability region. The diagram shown in Fig. 2 consists of 46,000 single measurements with a variation of $\Delta U_0 = 2.5$ V, $\Delta V_0 = 1.25$ V. The other experimental parameters such as creation period, electron current and acceleration voltage were held constant at the order of 10^{-3} in order to make sure that the initial conditions are the same for each data point. The background pressure of 10^{-9} mbar varied through the runs by less than 10 %. We choose 300 ms as time interval between the end of the ion creation and start of the extraction pulse.

Most prominent in Fig. 2 is the diagram from stored N_2^+. In addition, there exist overlapping stability areas from other ion species at the higher voltage side. As the detection settings and the timing gate are optimized for mass 28, the other masses get suppressed by factors of 10 (in the vicinity of the N_2^+-diagram) to 25 (at the end of the V_0-scale). For better visibility, the contrast and darkness in the diagram is enhanced strongly in those regions and also in the N_2^+-area where the ion number is low. So Fig. 2 does not contain information about real ion numbers. We discuss the actual number of trapped ions in Sect. 3.3. We identified the different ion masses by comparison with the theoretical stability diagrams and found coincidences for $m = 28$ amu (N_2^+/CO^+), $m = 32$ (O_2^+), $m = 40$ (Ar^+) and $m = 44$ (CO_2^+). These ions are expected as main components in the background gas. The borders of our experimental stability regions show a deviation smaller

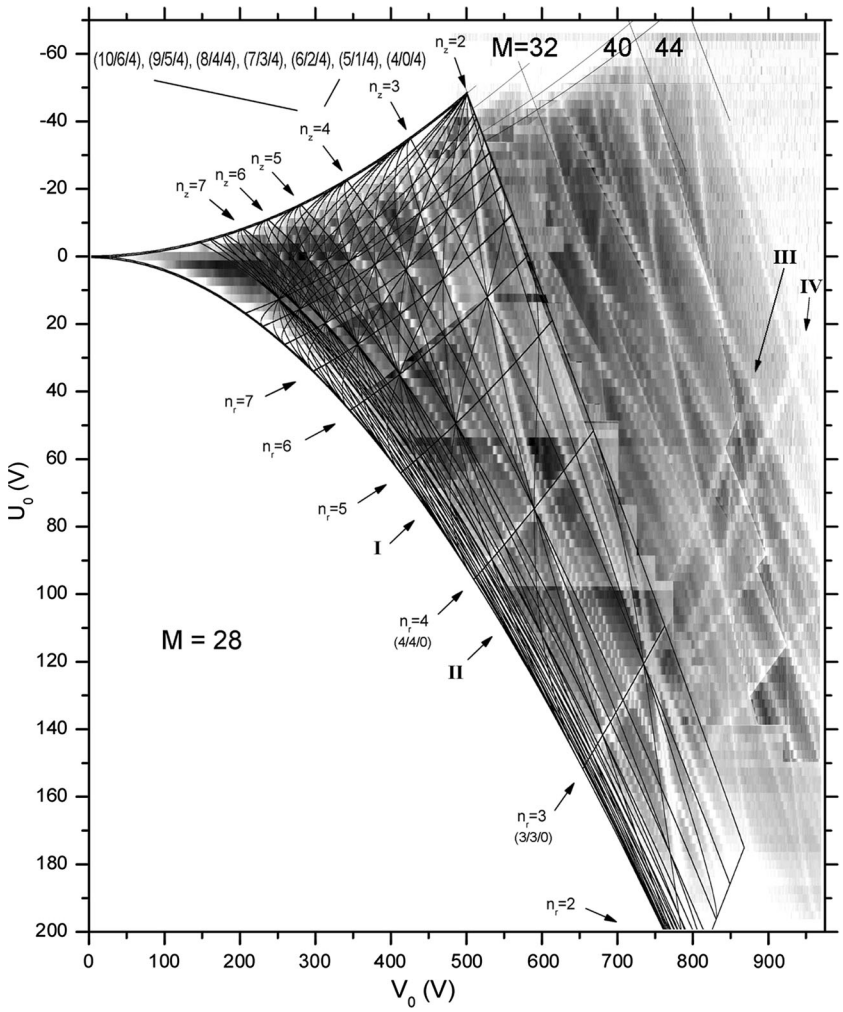

Fig. 2 Experimental high-resolution map of stored N_2^+. The theoretical boundaries of the stable region as well as the predicted nonlinear resonances are indicated by *solid lines*. The diagram is overlapping with higher mass stability regions for the mass numbers 32, 40 and 44. The labeling of the *lines* of motional instability in the *upper left corner* is ($N/n_r/n_z$). For the notion I, II, III and IV see text

than 2 % from the theoretical value, which is about the size of the uncertainty we obtained in calibrating the rf amplitude.

3.2 Nonlinear resonances

As evident from Fig. 2, we observe a number of lines where the detected ion number is greatly reduced. These are so-called nonlinear resonances [7] caused by nonharmonic components in the trapping potential as described in the introduction. We superimpose both the experimental and theoretical stability diagrams and directly identified the coefficients n_r, n_z as defined in Eq. (3) and consequently the order N of the unharmonic contribution which causes each individual instability. This is performed in Fig. 2 for N_2^+. Drawn are the resonances up to order $N = 10$ for $\kappa = 1$ according to Eq. (3).

We label the lines ($N/n_r/n_z$) following previous work in our group [10]. We denote in Fig. 2 the points where all lines of one particular n_r or n_z start and for $n_z = 4$ as example the different contributions of potential unharmonicities which lead to the instabilities starting at the same operating point.

In general, for all the masses, we see a good agreement with the theoretical expectations: uncoupled and sum resonances arising from low-order perturbations of the potential are strong, getting weaker with increasing resonance order N. We can identify nearly all of them up to $N = 9$ and some for $N = 10$. Resonances for $\kappa = 2$ are weak and barely visible. Resonances for $\kappa = 0$ are not seen at all; this is not unexpected since they have no coupling to the rf drive's frequency. Very weak $\kappa = 0$ might be expected when the coupling of radial and axial oscillations as always present in a nonharmonic trap leads to accidental energy increase in one of the modes which is sufficient for ion loss. Lines arising from low orders of the unharmonic potential part and with only radial component (e.g., (3/3/0)) can be observed to split in two lines for the same values of n_x and n_y, as a result of a violation of the radial symmetry of the trap. This holds also for higher-order components, but because of their relative weakness, it is difficult to observe.

Apart from those expected types of lines, we observe two weak parts of lines inside the overlapping mass 40/44 diagrams which fit to resonances arising from differences in the linear combinations of oscillation frequencies. A high resolution display of that area of the diagram in Fig. 3 shows the possible difference resonance lines indicated by white ovals and the fitting theoretical lines calculated for $M = 40$ amu. They correspond to a labeling (8/−3/5) and (9/−3/6). If one assumes those lines to belong to mass 44, the theoretical lines (8/−2/6) and (7/−2/5) would come similarly close to the experimental resonances. Difference

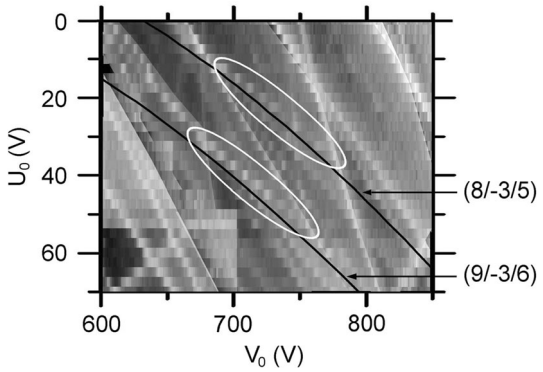

Fig. 3 Small part of Fig. 2 with theoretical difference resonances calculated for mass 40

instabilities have only been observed previously in case of pure radial-axial motion coupling [11]. It is somewhat surprising that such instabilities, particularly those arising from lower-order potential contributions, other than the observed ones seem not to appear in the diagram.

Additionally, we are left with four strong lines (I–IV), which do not fit to any of the lower perturbation orders for the observed ions. Attempts to ascribe these instabilities to perturbation by an additional rf field from an unknown source or by noise were unsatisfactorily: the 4 lines would require 4 different noise frequencies. Moreover, attempts to find combinations of numbers n_r and n_z to assign the lines to an order of an unharmonic part in the trapping potential lead to extremely high and unlikely orders, and the question would remain why lower orders which are in general much more likely to appear do not show up. It may well be that (I–IV) are caused by some kind of disturbing frequency source in our lab, but at this point, the cause of those instabilities remains unclear and needs further investigations.

The trapped ion number throughout the N_2^+-stability region in Fig. 2 varies by more than two orders of magnitude. We changed the contrast of the black-and-white picture in order to enhance the visibility of the nonlinear resonance lines. The information on the actual ion number will be considered in the following chapter.

3.3 Trapping capacity

We use the experimental data of 3.1 (upon which fig. 2 is based) to determine the trapped ion number. We concentrate on mass 28 and show the result in the 3D plots of Fig. 4: there are huge differences in the trap's capacity throughout the stability region, and we find the area of highest ion number to be much closer to the low-q region than in a previous measurement [12].

We now consider single horizontal scans through the stability diagram by varying V_0 in steps of 1.25 V and

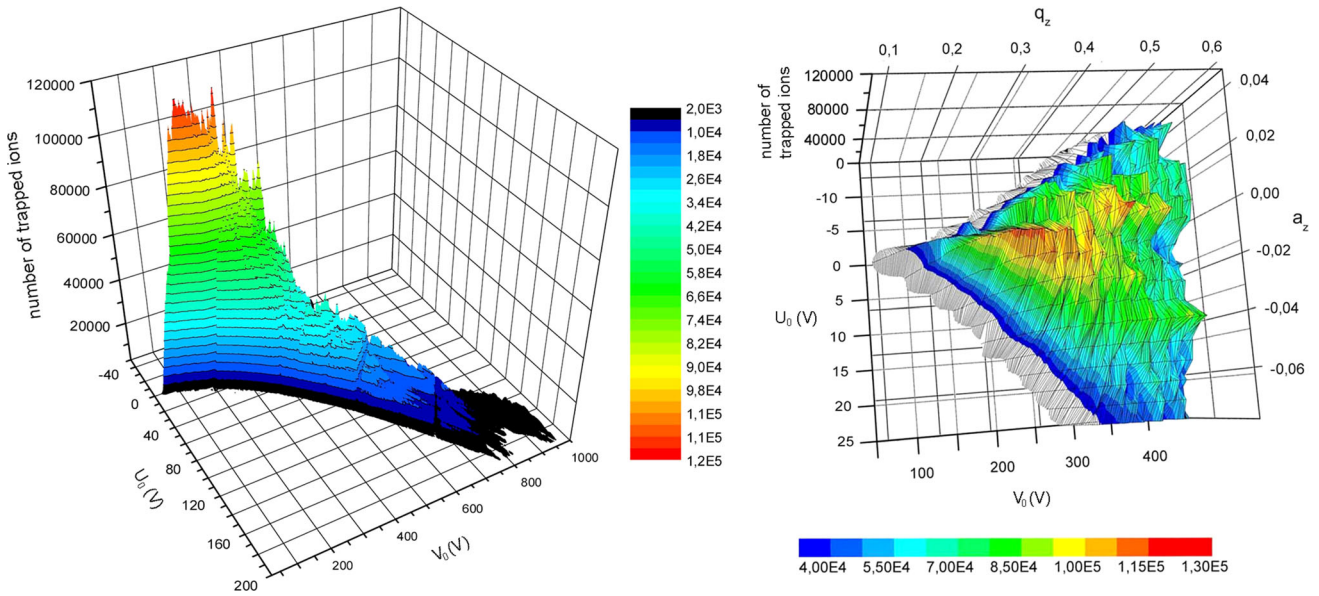

Fig. 4 3D plot of the ion numbers of Fig. 2 for mass 28 showing the whole diagram (*left*) and the part with the highest trapping capacity (*right*). The plot at the left seems to not contain resonance lines, but this is due to the point of view: at the low-V_0 side, the depth of the resonances is too small to be displayed here. But the *lines* (4/4/0) and (3/3/0) are easily visible

setting U_0 to zero. We have performed measurements at different pressures using helium and nitrogen as buffer gases. Figure 5 shows several of those scans with helium pressures varying between 5×10^{-8} and 8×10^{-6} mbar.

We observe a very strong shift in the parameters for maximum ion number and also a significant change of the overall ion number. Similar scans were made for nitrogen as buffer gas. The results for the trapping capacity as well as the parameters for maximum ion number as function of pressure for both buffer gases are displayed in Fig. 6. The observation can qualitatively be well understood. Increasing pressure leads to stronger damping and thus reduces the ion′s oscillation amplitude. At the same time, collisions lead to phase changes in the ion′s motion with respect to

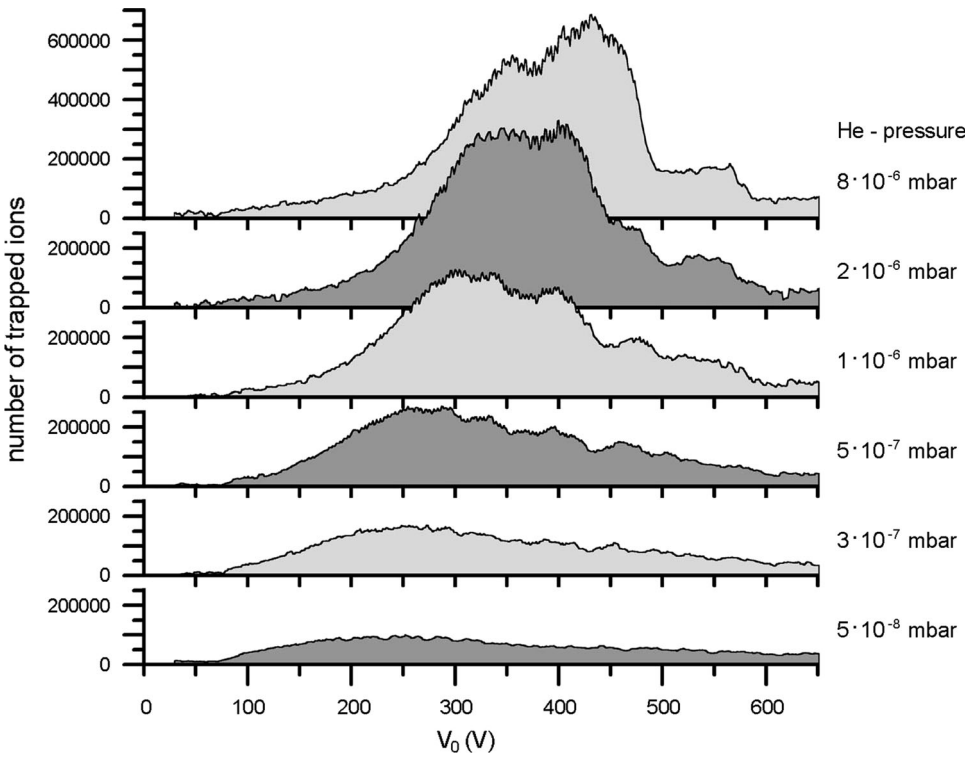

Fig. 5 V_0-scans through the stability diagram of N_2^+ at different Helium buffer gas pressures. The dc voltage across the trap was held at zero (creation time was 250 ms and trapping duration 300 ms, the error in pressure monitoring is about 10 %)

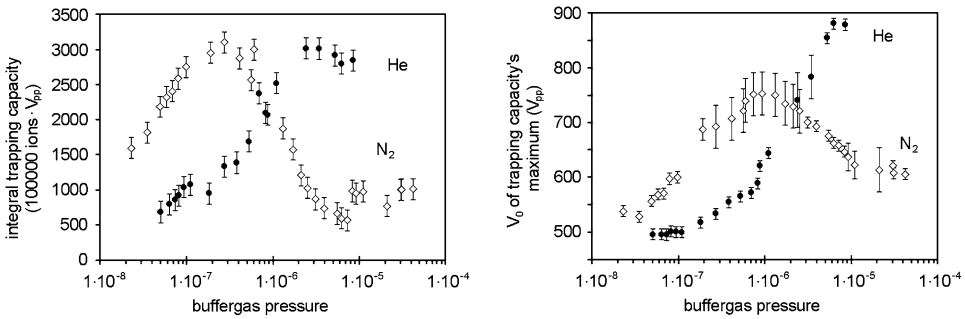

Fig. 6 *Left* change of the trapped ion number (integrated over the q-scans to average out the effects of nonlinear resonances) at different buffer gas pressure (Helium or Nitrogen). *Right* value of the rf amplitude V_0 for maximum trapped ion number as a function of the buffer gas pressure

the rf trapping field. At low pressures, the damping effects dominate, and at higher pressures, the phase changes lead to ion loss from the trap. This is particularly important when the ratio of the masses of ion and buffer gas atoms is small as discussed in detail by Major and Dehmelt [13]. This corresponds to the observation of Schwebel et al. [14]. Thus, it is obvious that the use of the light helium atoms allows much higher pressures for optimum trapping of ions with higher masses than helium.

Also the position of the trapping capacity's maximum is a result of the damping force of the buffer gas counteracting the rf heating by the trapping field which is particularly strong at high trapping field amplitudes. Increased damping by higher pressures allows operation at higher values of V_0 corresponding to deeper potential depth. This is limited at too high background pressures by the phase-changing collisions as mentioned above. Correspondingly, we find an optimum value for the trap's rf amplitude at different pressures depending on the buffer gas. In our experiments, we were limited in the background pressure to 1×10^{-5} mbar, and from the data in Fig. 6, we have to assume that the expected decrease in the ion number which we observe for N_2 appears at somewhat higher pressures for He.

3.4 Space charge shift and collective resonances in the stability diagram

An ion cloud can perform two types of movement resulting in two different types of resonances which we can distinguish: first, the ions can move individually. The ions near the center of the trap see a different effective trapping potential than the ions at the outer part of the cloud. The ion's oscillation therefore takes place in a broad frequency band, resulting in a broadened resonance. This type of resonance shifts with space charge to lower frequencies or in the stability diagram appears at higher trapping voltages to compensate for the space charge potential which can be seen as an additional dc voltage decreasing the trap's potential [14–16]. Second, at higher ion numbers, the trapping potential is weakened by the space charge potential, and the Coulomb interaction between the ions grows in importance and couples their motions. Then, the ions perform a collective motion—the center of mass motion. This results in a sharp resonance at the motional frequency of a single ion no matter how many ions are trapped. As long as there is only one ion species in the trap, there exists no space charge shift for that kind of resonance. The collective resonance needs a threshold for the ion number or excitation energy to appear [17, 18].

In order to investigate space charge effects, we repeat the horizontal scans through the stability diagram without buffer gas and vary the ion number by change of the creation time. As expected, the position of the nonlinear resonances within the stability region shifts with increasing ion number to higher values of the stability parameter q. We observe a shift of V_0 of about 10 V when the ion number is increased from 20,000 to more than 300,000 (Fig. 7). This is much smaller than the change of the capacity's maximum observed of more than 100 V and more than 200 V with nitrogen and helium as buffer gases, respectively (see Fig. 6). This indicates that damping by buffer gas has a big influence on the trapping capacity. In contrast, we did not observe a change of the oscillation

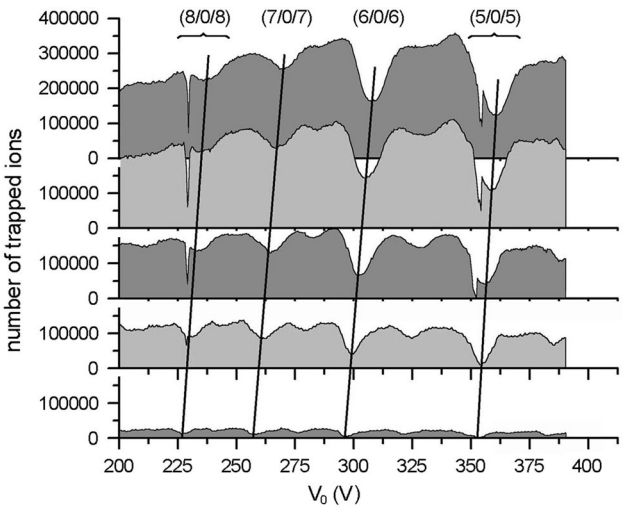

Fig. 7 Scans through the stability diagram of N_2^+ varying V_0 in steps of 0.5 V at $U_0 = 0{,}3$ V at a background pressure of $P = 1{\cdot}10^{-9}$ mbar. Space charge shift of the individual resonances (*black lines*) and narrow collective resonances can be observed

frequencies with buffer gas in the pressure range 5×10^{-8}–8×10^{-6} mbar. By varying the space charge, the oscillation frequencies change as expected: with the formulas derived by Fischer [15] and Meis [16], the calculated space charge shift matches our experimental data when assuming ion cloud radii of about 2.5 mm (Fischer) or 4 mm (Meis) which are reasonable values.

The narrow features near the trapping voltage amplitudes of 230 and 360 V appearing in Fig. 7 represent excitations of the center of mass resonance of the ion cloud. They are identified by the fact that the center of mass does not experience any space charge. In contrast, the positions of the resonances of the individual ions motion are shifted to higher values of the trapping voltage and are broadened. The voltages at which we observe the collective resonances are the same ones as for the individual resonances when having a small ion number. Those collective resonances have been previously observed only when the ion's motion was excited by an external drive field [17, 18]. Indication of the excitation of a collective resonance without an additional external rf field has been mentioned previously by Rettinghaus [19]. Here, we report them without ambiguity as side structure of the resonances at (8/0/8) and (5/0/5). The collective resonances only appear when having large ion numbers in the trap, indicating that a certain strength of the Coulomb interaction is necessary to couple the ion's motion. Previous investigations on the onset of externally excited collective resonances [18] showed a relation between ion number and the threshold excitation amplitude. At smaller ion numbers, higher amplitudes had been necessary. We therefore conclude that in our case, the energy transfer from the trapping field to the ion cloud via nonlinear coupling (Eq. 3) is at high ion densities sufficiently strong to start collective motions.

3.5 Collective resonances in the frequency spectrum

Collective resonances appear also by excitation of the ion cloud from additional rf fields applied to the trap electrodes. We apply an rf voltage of some mV amplitude to the trap's endcaps at fixed trapping voltages V_0 and U_0 during the storage period and repeat the creation-storage-detection cycles while changing the excitation frequency.

The frequency spectrum shows resonances at the ion's eigenfrequencies ω_r and ω_z as well as at linear combinations of those frequencies and the trapping field's frequency

$$\omega = |k\,\Omega + k_r\omega_r + k_z\omega_z|, \quad k = 0, 1, 2, \ldots \quad k_r,\ k_z = 0, \pm 1, \pm 2, \ldots \tag{4}$$

Each of these resonance lines consists of an individual and a collective resonance. Due to the quadrupole excitation, we expect to see strong ion motions with k_r, $k_z = \pm 2$, and the broken radial symmetry causes the ω_r resonances to split slightly.

As the strength of the resonances varies, not all of them appear in the typical low-resolution spectrum shown in Fig. 8.

When the trapping voltages are changed, the resonance lines in the spectrum move and occasionally some of them coincide with others. This happens when the trapping parameters hit a collective resonance in the stability diagram. For example, the resonances $3\omega_z$ and $\Omega - 2\omega_z$ would meet at the parameters of the resonance (5/0/5) in the stability region. In this case, coupling of the motional frequencies $3\omega_z = \Omega - 2\omega_z$ occurs and the resulting $5\omega_z = \Omega$ leads to the resonance order (5/0/5) following Eq. (3).

The collective resonances, which previously have been considered to be stationary, slightly seem to shift with ion number (Fig. 7). This shift is more obvious in the frequency spectrum (Fig. 9). It is smaller than the space charge shift of the individual resonance and can be explained by the space charge of the simultaneously stored ions of different mass. Those do not take part in the collective movement as their motional frequencies are different, but they change the effective potential of the trap. And as the N_2^+ molecular ions are created by background

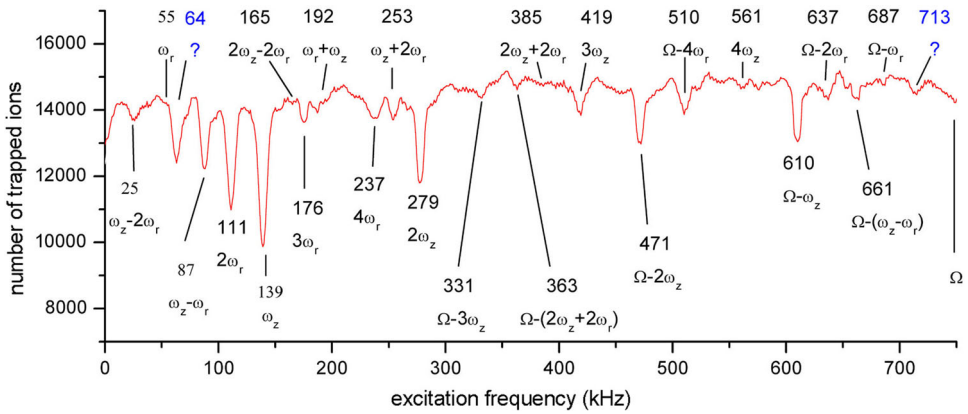

Fig. 8 Experimental frequency spectrum. Indicated frequencies of the resonances and allocations are for $m = 28$. Trapping parameters: $U_0 = -4.2$ V, $V_0 = 310.1$ V, creation and trapping duration both 300 ms, background gas pressure 3×10^{-9}mbar

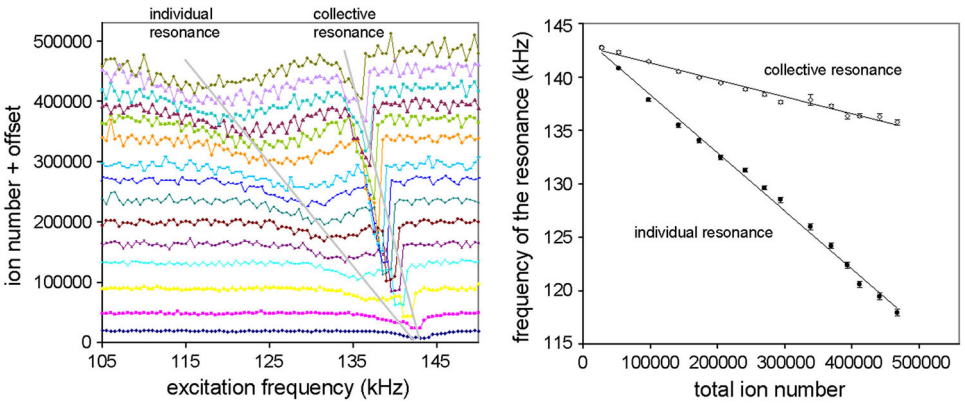

Fig. 9 Shift of the collective and individual resonance $2\omega_z$ at different ion numbers. Trapping parameters: $U_0 = 3$ V, $V_0 = 199$ V, $P = 2.6 \times 10^{-8}$mbar

gas ionization, a longer creation time also leads to a bigger amount of the other ("unwanted") ions (O_2^+, Ar^+, CO_2^+).

For further investigation of the collective (center of mass) resonances, we concentrate our studies on the line at $\omega = 2\omega_z$. In case of a single stored ion species, the frequencies of the collective resonances are independent of the ion number while the individual resonances shift by space charge as shown in Ref. [9, 18]. When different ion species are simultaneously stored, the collective resonance shifts as well, according to the space charge of the non-resonant ion species. Figure 9 shows this shift for N_2^+ ions in the presence of O_2^+, Ar^+ and CO_2^+ impurities.

As the individual resonance shows the total space charge shift and the collective resonance shows the space charge shift caused only by the "unwanted" ions, we can calculate their amount to be about 30 % of the total ion number. When we take this ratio, the measured N_2^+-ion number and the observed shift of the individual resonance and further consider that the space charge shift is mass dependent [16] (in our case mainly from O_2^+), we calculate the total space charge shift to $\delta\omega_z = 27$ (8) mHz/ion.

The shape of the collective resonances as shown in a high-resolution scan in Fig. 10 can be qualitatively understood: The resonance shape is a Lorentzian as long as the trap potential is a perfect quadrupole potential and the ions oscillate harmonically. In case of perturbation as caused by trap imperfections and by space charge, the resonance line becomes asymmetrical and tilted [20]. The direction of the asymmetry depends on the sign of the coefficients of the higher-order anharmonic potential contributions. In our case, the resonance shows a sharp edge at the low-frequency side for small ion numbers when the space charge is small and the trap asymmetry dominates. When the space charge potential increases with higher ion numbers, the line becomes at first more symmetrical and finally shows a sharp edge on the high-frequency side. We have to conclude that the sign of the anharmonic higher-order potentials is different when they arise from trap imperfection or from space charge.

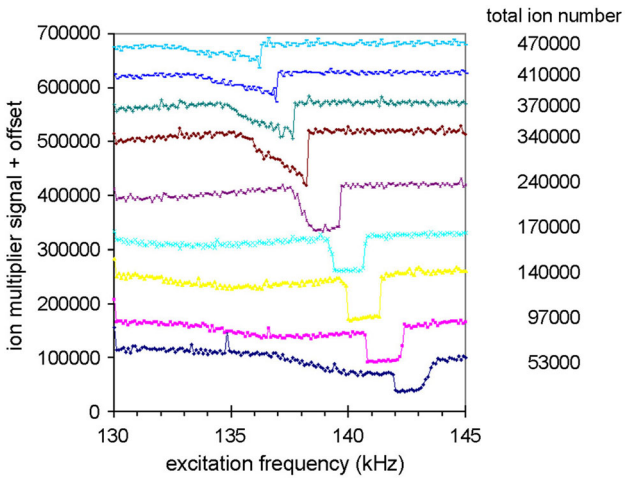

Fig. 10 High-resolution measurement of the $2\omega_z$ collective resonance of Fig. 9. The collective resonance changes its shape with the ion number. The gain of the ion multiplier has been increased in case of small ion numbers

For large higher-order potential contributions the resonance tilt of the anharmonic oscillator resonance becomes so big that at certain frequencies, the amplitude can assume two discrete and well-separated values. In case of continuous excitation of the ion cloud, this leads to a hysteresis when the direction of the exciting frequency sweep is changed and a sharp jump in the oscillation amplitude [8]. In our case, we do not excite the ions continuously, but at each frequency step, we start with a new ion cloud which then has no "memory" of the frequency scan direction. As a result, the amplitude of the ion's oscillation assumes statistically one of the two possible values, and we have a bistability in a certain frequency range as shown in Fig. 11.

Figure 12 shows a peculiar observation: Using storage durations between 200 and 2000 ms, we often see an additional "step" in the resonances. This corresponds to a similar observation by Holzki [9] within collective resonances and which is assumed to represent the instable intermediate state of a nonlinear resonance [20].

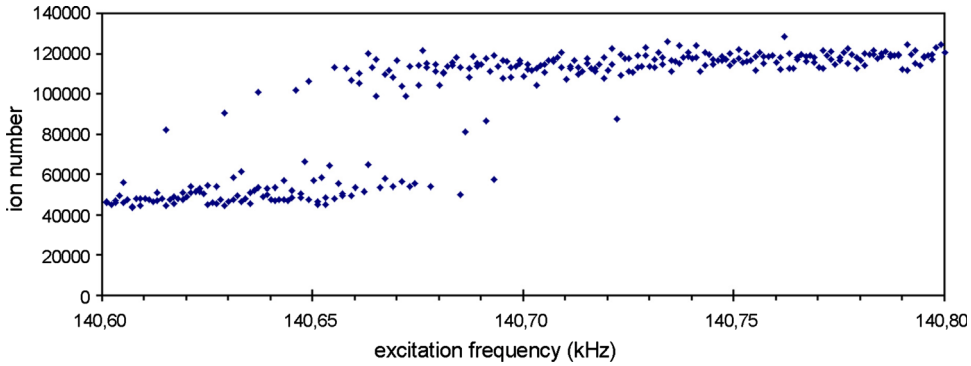

Fig. 11 High-resolution spectrum of the edge of the $2\omega_z$ resonance, showing the zone of bistability. Trapping parameters: $U_0 = 3$ V, $V_0 = 200$ V, $P = 2.7 \times 10^{-8}$mbar

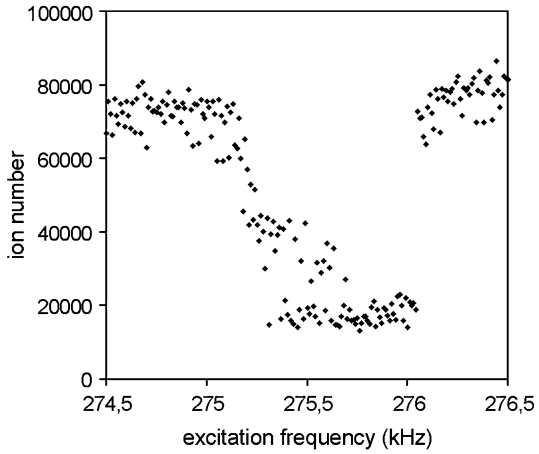

Fig. 12 Intermediate datapoints at the resonance $2\omega_z$ at a storage time of 300 ms. Trapping parameters: $U_0 = -4.2$ V, $V_0 = 310$ V, $P = 7 \times 10^{-9}$mbar

4 Conclusion

Our investigations on buffer-gas-cooled ion clouds of relatively large ion numbers and of different simultaneously stored ion species showed some interesting effects: damping by buffer gas results in a large change of the trapping characteristics in terms of storage capacity and optimum trapping parameters. The position of nonlinear resonances resulting from trap imperfections or space charge contributions to the trapping potential shifted with the ion number and was independent of the buffer gas conditions within our pressure range. For the first time, we show experimental data of collective resonances in the stability diagram without additional external excitation. Excitation of the stored ion's oscillation frequencies resulted in individual and center of mass resonances as observed earlier. As expected, the individual resonances shift with the ion number due to space charge. The center of mass resonances of a given ion species which so far are considered as independent of the ion number showed shifts when different ion species are stored simultaneously. This is attributed to the space charge potential from the other ions which also has an influence on the shape of the resonance. Our observations are of importance when the mass-dependent oscillation frequencies are used for high resolution mass measurements in Paul traps in the presence of different stored ion species. The high density of nonlinear resonances in the stability region may influence the observed ion number when dissociation or molecular formation takes place, and therefore, different ion species are trapped simultaneously.

Acknowledgments The experiments were supported by the Deutsche Forschungsgemeinschaft. We thank Stefan Krause for his providing programs for data taking and handling as well as Alexandros Drakoudis and Martin Söllner for their help and fruitful discussions.

References

1. R.E. March, R.J. Hughes, *Quadrupole storage mass spectrometry* (Wiley-Interscience, New York, 1989)
2. R.G. Cooks, G.L. Glish, S.A. Mc Luckey, R.E. Kaiser, Ion trap mass spectrometry. Chem. Eng. News **69**, 12 (1991)
3. R.E. March, in *Encyclopedia of analytical chemistry*, ed. by R.A. Meyers (Wiley, Chichester, 2000), pp. 11848–11872
4. J.F.J. Todd John, R.E. March, E. Raymond, *Quadrupole ion trap mass spectrometry*, 2nd edn. (Wiley-Interscience, New York, 2005)
5. Y. Wang, J. Franzen, The non-linear resonance ion trap, Part 3. multipole components in three types of practical ion trap. Int. J. Mass Spectrom. Ion. Proc. **132**, 155 (1994)
6. Y. Wang, J. Franzen, K.P. Wanczek, The non-linear resonance ion trap. Part 2. A general theoretical analysis. Int. J. Mass Spectrom. Ion. Proc. **124**, 125 (1993)
7. R. Alheit, S. Kleineidam, F. Vedel, M. Vedel, G. Werth, Higher order non-linear resonances in a Paul trap. Int. J. Mass Spectrom. Ion. Proc. **154**, I155 (1996)
8. M. Sudakov, D.J. Douglas, Linear quadrupoles with added octopole fields. Rapid Comm. Mass Spectrom. **17**, 2290 (2003)
9. Holzki M (1997) Untersuchung von gekoppelten nichtlinearen Oszillationen einer Ionenwolke in Ionenfallen, thesis, Mainz
10. R. Alheit, Th Gudjons, S. Kleineidam, G. Werth, Some observations on higher-order non-linear resonances in a Paul trap. Rapid Comm. Mass Spectrom. **10**, 583 (1996)
11. M. Vedel, J. Rocher, M. Knoop, F. Vedel, Evidence of radial-axial motion couplings in an rf stored ion cloud. Appl. Phys. B **66**, 191 (1998)
12. R. Iffländer, G. Werth, Optical detection of ions confined in a rf quadrupole trap. Metrologia **13**, 167 (1977)

13. F.G. Major, H.G. Dehmelt, Exchange-collision technique for the rf spectroscopy of stored ions. Phys. Rev. **170**, 91 (1968)
14. C. Schwebel, P.A. Möller, P.T. Manh, Formation et confinement d'ions multicharges dans un champ quadrupolaire a haute fréquence. Revue de Physique Appliquée T **10**, 227 (1975)
15. E. Fischer, Die dreidimensionale Stabilisierung von Ladungsträgern in einem Vierpolfeld. Z. Physik **156**, 1 (1959)
16. C. Meis, M. Desainfuscien, M. Jardino, Analytical calculation of the space charge potential and the temperature of stored ions in an rf quadrupole trap. Appl. Phys. B **45**, 59 (1988)
17. F. Vedel, M. Vedel, Nonlinear effects in the detection of stored ions. Phys. Rev. A **41**, 2348 (1990)
18. R. Alheit, X.C. Chu, M. Hoefer, M. Holzki, G. Werth, R. Blümel, Nonlinear collective oscillations of an ion cloud in a Paul trap. Phys. Rev. A **56**, 4023 (1997)
19. Rettinghaus G (1965) Nachweis niedriger Partialdrücke mit dem Ionenkäfig, Ph. D.-thesis, Bonn
20. L.D. Landau, E.M. Lifschitz, *Lehrbuch der theoretischen Physik, Bd. 1 Mechanik*, 9th edn. (Akademie-Verlag, Berlin, 1976)